The Transition from Refraction to Ultra-Small-Angle X-ray Scattering (USAXS) in a Laboratory Phase-Based X-Ray Microscope for Soft Tissue Imaging.

Michela Esposito[1,a)], Lorenzo Massimi[1], Ian Buchanan[1], Joseph D. Ferrara[2], Marco Endrizzi[1] and Alessandro Olivo[1]

[1]*Department of Medical Physics and Biomedical Engineering, University College London, Gower St, London WC1E 6BT, UK*
[2]*Rigaku Americas Corporation, 9009 New Trails Drive, The Woodlands, Texas 77381, US*

[a)]Corresponding author: michela.esposito@ucl.ac.uk

Abstract. We report on a laboratory-based x-ray microscope allowing for phase-contrast imaging of soft tissue samples. The used beam tracking approach allows retrieval of Ultra-Small-Angle X-ray Scattering (USAXS) or dark field alongside attenuation and differential phase. We show the dependence of the refraction and dark field signal on the size of the imaged features. The application of the technique to a biological sample is also demonstrated.

INTRODUCTION

Advances in cell and functional biology, together with the need for a faster and more accurate histology in cancer diagnostics, has created the need for imaging mm-sized tissue samples with micron and sub-micron resolution to identify structures, cell types, and their relationship. To address these needs, we have developed a low-energy x-ray phase-based x-ray microscope [1, 2] using intensity-modulation masks for single-shot retrieval [3] of three contrast channels, namely transmission, refraction, and Ultra-Small-Angle X-ray Scattering (USAXS) or dark field. We have experimentally demonstrated [1] how the spatial resolution of the microscope is entirely determined by the mask aperture width and, unlike other x-ray imaging modalities, does not depend on source size and detector pixel pitch, so long as some general conditions on system design are met [1, 2]. This result facilitates the implementation of a multi-resolution microscope through the use of different size masks, while no additional requirements are imposed on source and detector.

Ultra-Small-Angle X-ray Scattering (USAXS) or dark field signal, originating from refraction of unresolved micro-structures below the resolution limit of the imaging system [4], allows us to explore samples below this limit through identification and possible quantification of microscopic structures. The capability to detect sub-pixel microscopic structures has been demonstrated for a number of phase-based imaging modalities including analyser-based imaging [5], grating interferometry [6], edge-illumination [7, 8], and beam tracking [3].

In this paper we report on the capability of the x-ray microscope to access the dark field signal at sub-micron scale and on how the refraction signal transitions into scattering. Additionally, we report on an exemplar image of a biological sample where refraction and scattering signal co-exist.

MATERIALS AND METHODS

The laboratory set-up used in this work consists of a rotating anode x-ray source, a monochromator selecting the Cu K_α lines ($\approx$ 8 keV) and focusing the beam to a 350 μm spot size. The x-ray beam is shaped into an array of beamlets by an intensity modulation mask (see Figure 1), consisting of an unsupported Au layer comprising 2-μm-wide slits and a 19 μm periodicity. The sample is placed as close as possible to the mask and a propagation distance of 15 mm

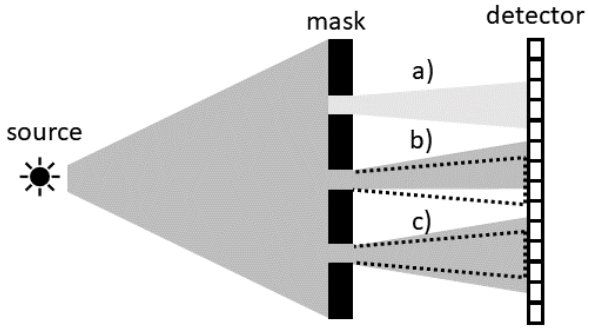

FIGURE 1. A schematic diagram of the beam tracking principle: an incoherent beam is shaped into an array of beamlets which are subjected to attenuation *(a)*, refraction *(b)* and scattering *(c)* when a sample is introduced. The dotted beamlets represent the reference beamlets in the absence of a sample.

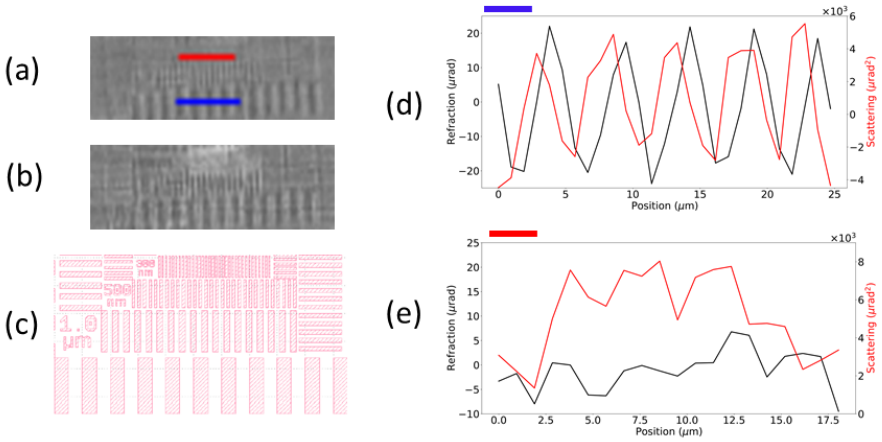

FIGURE 2. Refraction *(a)* and scattering *(b)* images of the bar pattern schematically shown in *(c)*.*(d)* and *(e)*: intensity profiles for refraction (black) and scattering (red) images for the blue and red region of interest indicated in *(a)*, corresponding to bar widths of 2500 and 500 nm, respectively.

is used between sample and detector. The detector, through a standard optical configuration [2], offers an effective 1.1 μm pixel pitch.

Sample properties are retrieved through fitting of the shaped beamlets with and without a sample in place. Figure 1 shows how the introduction of a sample modifies the shaped beamlets. Depending on the sample properties, a beamlet can be attenuated (beamlet a in Figure 1), providing an estimate of the attenuation coefficient μ (with $\mu = 2k\beta$). It can be subjected to a transverse shift due to refraction (beamlet b in Figure 1), resulting from the real part of the unit decrement of the sample's refraction index ($n = 1 - \delta + i\beta$). Additionally, when a sample includes features on a length-scale below the system resolution, unresolved refraction results in a broadening of the beamlets (beamlet c in Figure 1). Further details on the retrieval procedure can be found in [1, 3].

In order to link the refraction and scattering signals with feature size, a bar pattern was used as test object. The bar pattern, schematically shown in Figure 2 *(c)* consists of 800-1000-nm-thick Au bars placed on a SiN_3 membrane in a series of patterns with half-pitches of 2500, 1000, 500 and 300 nm. The sample was exposed for 50 frames of 10 s each and dithered in 20 steps of 0.95 μm, corresponding to a mask period. With dithering, we refer to the stepping of the sample in a series of increments smaller than the mask period, thus creating a series of frames that are then recombined to create an image in which the spatial resolution is independent on the mask period [9]. A thin section of rabbit articulation, including cartilage, bone marrow, and trabecular bone was also imaged with the same experimental

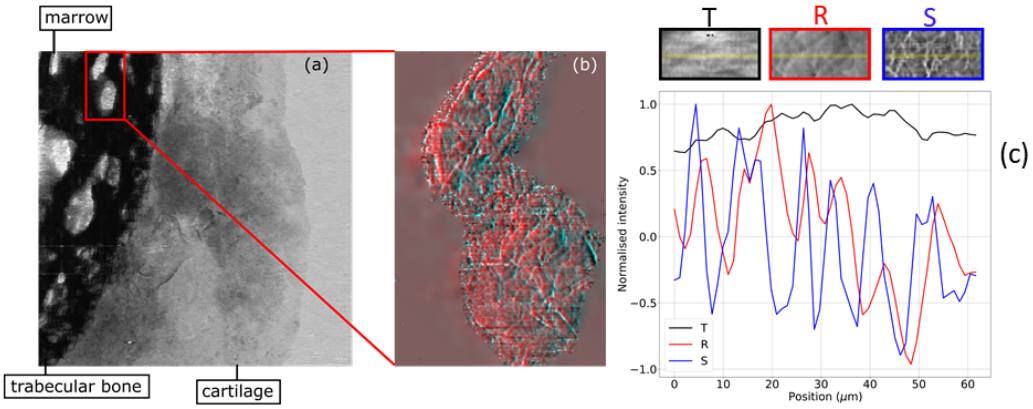

FIGURE 3. Transmission image of a thin slice of rabbit articular tissue *(a)*. The area surrounded by the red box is magnified and shown in panel *(b)* for the co-registered refraction (red) and scattering (cyan) images after segmentation and masking of the trabecular bone. *(c)*: transmission (black, T), refraction (red, R) and scattering (blue, S) images of a region inside the bone marrow area. Intensity profiles corresponding to the yellow lines are also shown.

parameters as detailed above.

RESULTS AND DISCUSSION

Retrieved refraction and scattering signals for the bar pattern are shown in Figure 2 *(a)* and *(b)*. The largest features (2.5 μm) are resolved in both contrast channels, in agreement with a resolution limit of 2 μm given by the mask slits' width as reported in [1]. In the refraction channel, the modulation of the 1 μm feature size appears reduced and affected by aliasing. For feature sizes well below the system resolution limit (500 and 300 nm), individual bars are not resolved in any of the two contrast channels. However, while we do not observe a refraction signal, the scattering signal is positive throughout the region corresponding to sub-micron feature sizes. Intensity profiles through the 2.5 μm and 500 nm bars are shown in Figure 2 *(d)* and *(e)*, corresponding to the region highlighted in blue and red respectively. The profiles for the largest features size show the capability of the system of resolving features larger than the mask slit widths. At smaller feature sizes, while the refraction profile is compatible with zero, the scattering peaks to a positive value for feature smaller than the system resolution.

A demonstrator image in the life-sciences is reported in Figure 3, showing an area of a rabbit knee. The retrieved transmission image (panel *(a)*) shows different articular tissues including trabecular bone, and cartilage. A region of interest comprising bone and bone marrow is shown in the co-registered image of inset *(b)*, after bone segmentation, where refraction is shown in red and scattering in cyan. Different areas of the sample exhibit signal in different channels, suggesting the complementarity of the different contrast mechanisms. Intensity profiles taken through a small region of the bone marrow containing vessel-like structures (Figure 3 *(c)*) compares the three contrast channels provided by this technique. Only a fraction of the vessels visible in the refraction image appear in transmission. This is due to the inherently lower contrast carried by the imaginary part of the refraction index compared to real part [10]. Additionally, strong scattering peaks associated with the vessels network are visible.

ACKNOWLEDGMENTS

Research reported in this publication was supported by the National Institute of Biomedical Imaging and Bioengineering of the National Institutes of Health under Award Number R01EB028829. The content is solely the responsibility of the authors and does not necessarily represent the official views of the National Institutes of Health. This project has received funding from the European Union's Horizon 2020 research and innovation programme under Grant Agreement No. 777222. Additional support was received from EPSRC (grants EP/T005408/1, EP/P023231/1 and EP/M028100/1). AO was supported by the Royal Academy of Engineering under their "Chairs in Emerging Technologies" scheme (CiET1819/2/78).

REFERENCES

[1] M. Esposito, L. Massimi, I. Buchanan, J. D. Ferrara, M. Endrizzi, and A. Olivo, Applied Physics Letters **120**, p. 234101 (2022).

[2] M. Esposito, L. Massimi, I. Buchanan, J. D. Ferrara, M. Endrizzi, and A. Olivo, "Test and optimization of a multi-modal phase-based x-ray microscope for soft tissue imaging," in *Medical Imaging 2022: Physics of Medical Imaging*, Vol. 12031 (SPIE, 2022), pp. 1 – 7.

[3] F. A. Vittoria, G. K. N. Kallon, D. Basta, P. C. Diemoz, I. K. Robinson, A. Olivo, and M. Endrizzi, Appl. Phys. Lett. **106**, p. 224102 (2015).

[4] C. M. Slack, Phys. Rev. **27**, 691–695 (1926).

[5] L. Rigon, H.-J. Besch, F. Arfelli, R.-H. Menk, G. Heitner, and H. Plothow-Besch, Journal of Physics D: Applied Physics **36**, A107–A112 (2003).

[6] F. Pfeiffer, M. Bech, O. Bunk, T. Donath, B. Henrich, P. Kraft, and C. David, Journal of Applied Physics **105**, p. 102006 (2009).

[7] M. Endrizzi, P. C. Diemoz, T. P. Millard, J. Louise Jones, R. D. Speller, I. K. Robinson, and A. Olivo, Appl. Phys. Lett. **104**, p. 024106 (2014).

[8] P. Modregger, M. Endrizzi, and A. Olivo, Applied Physics Letters **113**, p. 254101 (2018).

[9] P. C. Diemoz, F. A. Vittoria, and A. Olivo, Opt. Express, OE **22**, 15514–15529 (2014).

[10] M. Endrizzi, F. A. Vittoria, P. C. Diemoz, R. Lorenzo, R. D. Speller, U. H. Wagner, C. Rau, I. K. Robinson, and A. Olivo, Opt. Lett., OL **39**, 3332–3335 (2014).